Electron. Mater. Lett., Vol. 12, No. 2 (2016), pp. 219-223
DOI: 10.1007/s13391-015-5352-y

Analytical Investigation of Carrier Concentration Effect on One-Dimensional Graphene Nanoscroll

M. J. Kiani,[1,*] E. Akbari,[2] F. Rahmanian Kooshkaki,[3] and A. Zeinalinezhad[4]

[1]Faculty of Electrical and Computer Engineering, Hakim Sabzevari University, Sabzevar, 9617976487, Iran
[2]Institute of High Voltage & High Current, Faculty of Electrical Engineering, Universiti Teknologi Malaysia, Johor Bahru, 81310, Malaysia
[3]Department of Computer, Khafr Branch, Islamic Azad University, Khafr, Iran
[4]Chemistry Department, Anar Branch, Islamic Azad University, Anar, Iran

(received date: 7 September 2015 / accepted date: 10 November 2015 / published date: 10 March 2016)

In recent years, carbon nanoscrolls (CNSs) that have a tubular structure similar to that of the open multi-wall carbon nanotube have received significant attention. Graphene nanoscrolls (GNSs) have also attracted significant attention, owing to their unique properties. These nanoscrolls are obtained by systematically winding graphene sheets into a spiral, and are expected to have high mechanical strength, high carrier mobility, and high thermal conductivity. In the present work, an analytical model was used to determine the band energy of (16,0) GNS, and the normalized Fermi energies in the degenerate and non-degenerate regimes are modeled. The model revealed that degenerate and non-degenerate approximations can be used for normalized Fermi energies higher than 3 and lower than -3, respectively.

Keywords: graphene nanoscroll, carrier concentration, non-degenerate regime, degenerate approximations, analytical model

1. INTRODUCTION

In recent years, the properties of carbon nanomaterials such as carbon nanotubes (CNTs) and graphene have been extensively investigated, and many potential applications of these materials have been explored; these applications include supercapacitors, hydrogen storage, and MOSFETs.[1-5] A novel and remarkable carbon nanomaterial, referred to as graphene nanoscroll (GNS), has also been explored.[6-8]

This material (i.e., GNS) has the potential to replace silicon in many electronic applications such as computers, televisions, cell phones, and other typical silicon-based technology. Many studies have focused on the application of nanoscrolls, which are especially useful as energy storage devices such as batteries and supercapacitors.[6,9,10] Unlike single-walled carbon nanotubes (SWCNTs), GNS is a spirally wrapped graphene sheet.[1]

*Corresponding author: kianiph@gmail.com

However, CNG is spirally wound from a two-dimensional (2D) graphene sheet into a 1D tubular structure, as shown in Fig. 2, and is therefore similar to the "Russian-Rolled" multi-walled carbon nanotube (MWCNT).[10,12,13] CNSs have attracted considerable attention as an open MWCNT-like tubular structure.[13-16] In fact, this material can be systematically wound into a spiral by twisting 2D graphene sheets.[2] Spirally wrapped GNSs are expected to inherit excellent properties from both graphene and CNTs. These properties result from the individual topological structure, high mechanical strength, high carrier mobility, and high thermal conductivity of the GNC.[18-20]

The Van Der Waals interactions between the inner and outer surfaces of graphene in the GNS, are significantly lower than those of MWCNT and graphene nanoribbon carbon-based materials.[3] As such, the electronic band structure and phonon dispersion of GNS may differ from those of MWCNTs and graphene nanoribbons. Several studies, focused on the use of GNS for energy and hydrogen storage, have considered the role of the scroll topology and

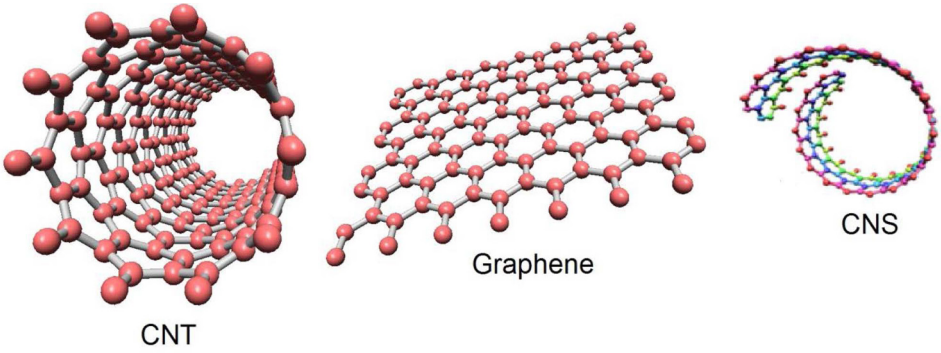

Fig. 1. Structural representations of graphene, CNT, and carbon nanoscroll (CNS).

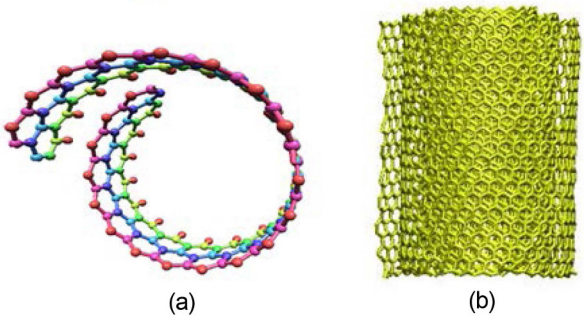

Fig. 2. (a) Spirally grown graphene referred to as graphene nanoscrolls (GNS) and (b) Top view of the GNS.

corresponding variable intra-layer distance.[20,22] For example, the high-surface-area flexible core enables the use of GNSs for hydrogen and energy storage in supercapacitors or batteries.[4] Electrical-transport measurements have indicated that the resistance of GNSs is temperature-dependent.[3] In addition, GNSs have various morphologies such as armchair (n, n), zigzag (n, 0), and chiral (n, m).[5] These materials differ from single-walled nanotubes (SWNTs), which have a chiral morphology only, as in the case of a small-gap semiconductor or metallic, for which n-m is a multiple of 3. However, the energy gap of GNSs varies significantly with the inner radius, thereby resulting in size-dependent properties.[6]

Therefore, in this study, the carrier concentration of the zigzag GNS (ZGNS) (16,0) is modeled and the dependence of the electronic properties on the structural parameters is examined. The corresponding one-dimensional (1D) density of states (DOS) is presented, based on the approximation of the energy dispersion relation for θ=1.9242.

2. MODEL

The nearest neighbor tight binding (NNTB) energy model of graphene, developed by Chen,[22,24] is used in this work.

$$E = \pm t\left(1+4\cos\left(\frac{\sqrt{3}ka_{cc}}{2}\right)\cos\left(\frac{j\pi}{n}-\frac{\theta}{2n}\right)+\left(4\cos^2\left(\frac{j\pi}{n}-\frac{\theta}{2n}\right)\right)\right)^{1/2} \quad (1)$$

where t, the nearest neighbor C-C overlap energy, typically ranges from 2.5 - 3.2 eV. In the present study, a value of 2.5 eV was chosen for t, based on Chen's work; $a = \sqrt[2]{3} * a_{cc}$ is the length of the basis vector, i.e., the Bravais lattice constant. The 1D energy dispersion of the GNS (16,0) is modeled by using Equation (2) and the resulting behavior of its small energy band gap and gain DOS of ZGNS (16,0) was examined.

$$E = \pm t\left\{5+4\cos\left(\frac{3ka_{cc}}{2}\right)\right\}^{1/2} \quad (2)$$

The Taylor expansion series is applied to the assumed ZGNS (16,0) energy equation, as the first sub-band is considered in the degenerate limit. As Fig. 3 shows, the modified energy band has a parabolic shape, as in the case of a 1D material.

$$E = \pm t\left(5-\frac{3a_{cc}^2k^2}{4}\right) \quad (3)$$

where k is the wave vector component around the circumferential direction, which is quantized by the periodic boundary condition. Therefore, the derivation of the energy band structure and the density of states for ZGNS is very useful in gaining insights into the corresponding electrical properties. Other device-physics parameters can also be determined, based on this work. The shape- and diameter-dependent electronic properties of the GNS are attributed to its open edges and no-cap structure.[7]

In fact, the inter-planar distance may vary significantly because the structure is open at both ends, and hence, the GNSs are especially sensitive to doping or intercalation.[17,25] The electronic and optical properties of the GNSs can be determined by performing ab initio calculations based on density-functional theory and local density approximation, which describe the ground-state properties of the CNSs.[26,27]

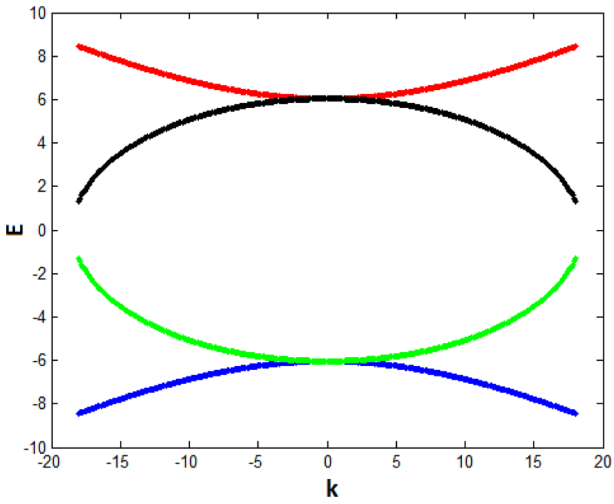

Fig. 3. The parabolic band structure of ZGNS (16,0).

Theoretical predictions indicate that ZGNS (16,0) altered the sub-band spacing owing to the ZGNS overlapping layer (Van Der Waals interaction between layers) and periodic increments of the radius. The DOS of the ZGNS is determined by differentiating the energy, with respect to k. Setting equation (3) equal to equation (1), rearranging, and performing the differentiation ($\partial E/\partial k$) leads to the following expression:

$$dE = \pm\left(\frac{3ta_{cc}^2\pi}{l}\left(\frac{4E}{3ta_{cc}^2}+\frac{20}{3ta_{cc}^2}\right)\right)^{1/2} dn \tag{4}$$

By rearranging equation (4), the DOS per spin per valley of the 1D ZGNS, is determined from:

$$DOS = \frac{dn}{LdE} = \pm\left(\frac{1}{3ta_{cc}^2\pi}\left(\frac{4E}{3ta_{cc}^2}+\frac{20}{3ta_{cc}^2}\right)\right)^{-1/2} \tag{5}$$

The carrier density is then obtained by rearranging the DOS; n corresponds to the number of possible carriers and L is the length of the conductance channel. The carrier concentration is therefore given as:

$$n = \pm\int \frac{1}{1+e^{\frac{E-E_F}{KT}}}\left(\frac{1}{3ta_{cc}^2\pi}\left(\frac{4E}{3ta_{cc}^2}+\frac{20}{3ta_{cc}^2}\right)\right)^{-1/2} dE \tag{6}$$

This concentration can be simplified by using the well-established Fermi integrals, and is given as follows:

$$n = \left(\frac{4}{9t^2a_{cc}^4\pi}\right)(K_BT)^{1/2}\Im_{-1/2}(\eta) \tag{7}$$

The carrier concentration of ZGNS (16,0), as determined from equation (7), is shown in Fig. 4.

The non-degenerate energy levels at distances of more than $3k_BT$ from either the conduction or valence band edge are manifested as a band gap at the Fermi level. In the case of a semiconductor, the Fermi level is located less than $3k_BT$ away from the conduction and the valence bands, or within a band, as shown in Fig. 5.

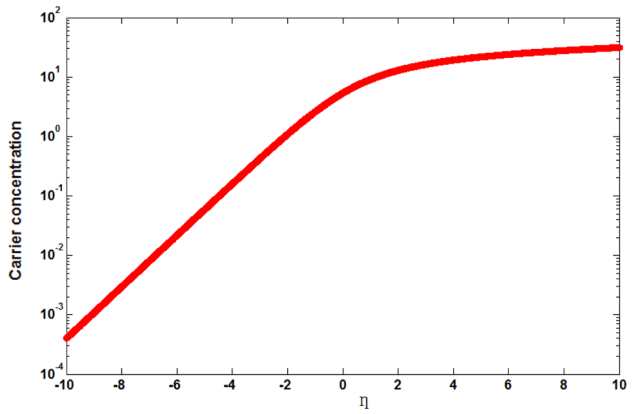

Fig. 4. The carrier concentration of the first sub-band of ZGNS (16,0) at $\theta = 1.9242$.

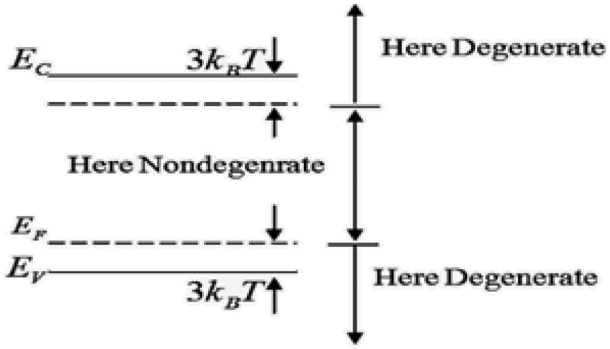

Fig. 5. Compression of the degenerate and non-degenerate regimes.

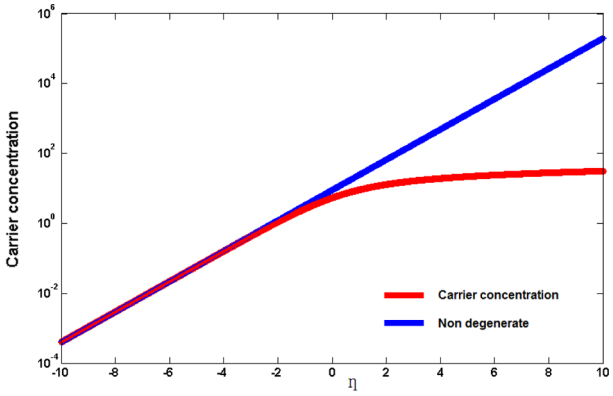

Fig. 6. Comparison of the carrier concentration of the ZGNS (16,0) at the first sub-band Fermi-Dirac integral and the non-degenerate regimes in the parabolic region.

In other words, the Fermi integral in this regime can be replaced by an exponential function, which is given as:

$$n_{ND} = \left(\frac{4}{9t^2a_{cc}^4\pi}\right)(K_BT)^{1/2}e^{\eta} \tag{8}$$

Equation (8) reveals that the carrier concentration of the non-degenerate states is a function of the thermal energy, and hence the number of carriers in this regime varies with the temperature. In Fig. 6, the non-degenerate states have normalized Fermi energies of <–3.

The approximation of the nano-scale regime will play an important role in determining the carrier concentration. The degeneracy of ZGNS can be determined by using the Fermi probability function, which is given as:

$$f(E) = \frac{1}{\exp\left(\frac{E-E_F}{k_B T}\right)+1} \tag{9}$$

In the degenerate regime, $E-E_F<3k_{BT}$ and therefore, $f(E)=1$, whereas $E-E_F>3k_{BT}$ in the non-degenerate regime and hence:

$$f(E) = \exp\left(\frac{E_F-E}{k_{BT}}\right) \tag{10}$$

In other words, the concentration of electrons in the conduction band exceeds the density of states; the Fermi energy lies within the conduction band as shown in Fig. 7. The expression $\exp(x-\eta)$ can be neglected in this regime, owing to the very small magnitude of $(x-\eta)$.

$$n_D = \left(\frac{4}{9t^2 a_{cc}^4 \pi}\right)\left(\frac{\frac{E_F-E_g}{K_B T}K_B T}{\pi}\right)^{1/2} \tag{11}$$

The degenerate limit carrier concentration is therefore independent of the thermal energy, and hence the temperature.

In Fig. 7, normalized Fermi energies of >3 correspond to the degenerate approximation of (16,0) GNS.

A comparison of the total carrier concentration, and the concentration of the degenerate and non-degenerate regimes is shown in Fig. 8. As the figure shows, the non-degenerate

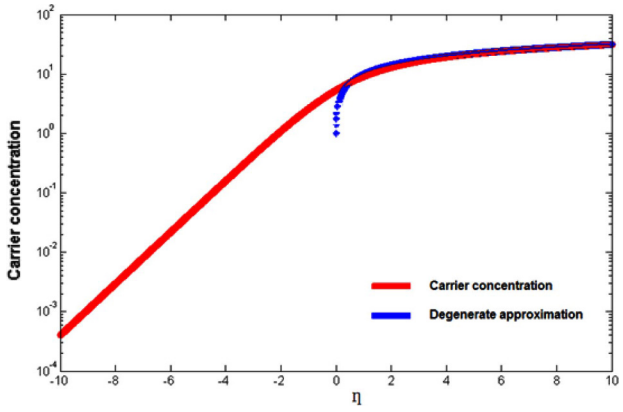

Fig. 7. Comparison of the carrier concentration of the ZGNS (16,0) at the first sub-band Fermi-Dirac integral and the degenerate regimes in the parabolic region.

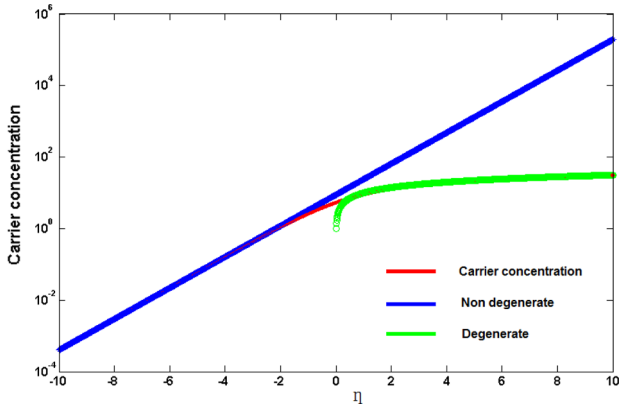

Fig. 8. Comparison of the carrier concentration (n) of the degenerate (nd) and non-degenerate (nnd) states.

and degenerate regions have carrier concentrations that occur at normalized energies (h) ranging from 10 to −3 and −3 to +10, respectively; h is the ratio of the Fermi and the thermal energies.

3. CONCLUSIONS

The 1D band energy, which gives rise to unique electrical properties such as high mechanical strength, high carrier mobility, and high thermal conductivity, of CNSs was discussed. The study focused on GNS (16,0) and an analytical model of the band energy was presented. In addition, the carrier concentration as a basic parameter of both the degenerate and non-degenerate regimes was explored. The model revealed that degenerate and non-degenerate approximations can be used for normalized Fermi energies higher than 3 and lower than -3, respectively. Furthermore, the carrier concentration of the non-degenerate regime varies with the thermal energy, whereas the concentration of the degenerate region is independent of the thermal energy.

ACKNOWLEDGEMENTS

The authors gratefully acknowledge the financial support from the Research Management Center of Hakim Sabzevari University for providing an excellent research environment, where this work could be completed.

REFERENCES

1. M. J. Kiani, F. K. Harun, S. N. Hedayat, and E. Akbari, *J. Comput. Theor. Nanos.* **10**, 1338 (2013).
2. M. J. Kiani, Z. Zamani, and A. Hosainzadeh, *J. Comput. Theor. Nanos.* **11**, 1453 (2014).
3. M. Rezaei-Sameti, *Quantum Matter* **2**, 396 (2013).
4. E. Akbari, Z. Buntat, and A. Enzevaee, *Electron. Lett.* **51**,

1092 (2015).
5. E. Akbari, Z. Buntat, E. Shahraki, and R. Parvaz, *J. Biomater. Appl.* 0885328215585682 (2015).
6. A. K. Schaper, H. Hou, M. Wang, Y. Bando, and D. Golberg, *Carbon* **49**, 1821 (2011).
7. D. Roy, E. Angeles-Tactay, R. J. C. Brown, S. J. Spencer, T. Fry, T. A. Dunton, and M. J. T. Milton, *Chem. Phys. Lett.* **465**, 254 (2008).
8. V. R. Coluci, S. F. Braga, R. H. Baughman, and D. S. Galvao, *Mater. Res. Soc. Symp. P.* **885**, 153 (2006).
9. T. K. Townsend, E. M. Sabio, N. D. Browning, and F. E. Osterloh, *Chemsuschem* **4**, 185 (2011).
10. T. S. Li, M. F. Lin, and J. Y. Wu, *Philos. Mag.* **91**, 1557 (2011).
11. S. F. Braga, V. R. Coluci, S. B. Legoas, R. Giro, D. S. Galvao, and R. H. Baughman, *Nano Lett.* **4**, 881 (2004).
12. K. Katagiri, A. Shimizu, T. Imanishi, T. Sato, N. Nakama, and A. Kakitsuji, *Sumitomo Presicion Prod. Co. Ltd*. (2008).
13. Y. Gao, X. Q. Chen, H. Xu, Y. L. Zou, R. P. Gu, and M. S. Xu, *Carbon* **48**, 4475 (2010).
14. P. Viel, X. T. Le, V. Huc, J. Bar, A. Benedetto, and A. Le Goff, *J. Mater. Chem.* **18**, 5913 (2008).
15. Y. Kuroda, K. Ito, K. Itabashi, and K. Kuroda, *Langmuir* **27**, 2028 (2011).
16. M. A. Bizeto and V. R. L. Constantino, *Micropor. Mesopor. Mat.* **83**, 212 (2005).
17. D. Xia, Q. Z. Xue, J. Xie, H. J. Chen, C. Lv, F. Besenbacher, and M. D. Dong, *Small* **6**, 2010 (2010).
18. J. Zheng, H.T. Liu, B. Wu, Y. L. Guo, T. Wu, and G. Yu, *Adv. Mater.* **23**, 2460 (2011).
19. X. H. Shi, Y. Cheng, N. M. Pugno, and H. J. Gao, *Appl. Phys. Lett.* **96**, 053115 (2010).
20. Z. Zhang and T. Li, *Appl. Phys. Lett.* **97**, 081909 (2010).
21. Y. Chen, J. Lu, and Z. X. Gao, *J. Phys. Chem. C* **111**, 1625 (2007).
22. X. Shi, N. M. Pugno, and H. Gao, *J. Comput. Theor. Nanos.* **7**, 517 (2010).
23. M. Lundstrom and J. Guo, Springer (2006).
24. B. F. Habenicht, O. N. Kalugin, and O. V. Prezhdo, *Nano. Lett.* **8**, 2510 (2008).
25. E. K. Yu, D. A. Stewart, and S. Tiwari, *Phys. Rev. B* **77**, 195406 (2008).